Earth and Planetary Science
https://journals.nasspublishing.com/index.php/eps

ARTICLE

Unraveling the Volcanic Structure of Oceanic Islands—Gravity Survey of Socorro Island, Revillagigedo Archipelago, Mathematician Ridge, Pacific Plate

Julio A. Pavón-Moreno [1] ***, Jaime Urrutia-Fucugauchi*** [2,3*] ***, Ligia Pérez-Cruz*** [2,3,4] ***, Marisol Escorza-Reyes*** [1]

[1] *Facultad de Ingeniería, Universidad Autónoma del Carmen, Carmen 24180, Mexico*

[2] *Programa Universitario de Perforaciones en Océanos y Continentes, Instituto de Geofísica, Universidad Nacional Autónoma de México, Mexico City 04510, Mexico*

[3] *Instituto de Investigación y Estudios Avanzados Chicxulub, Parque Científico Tecnológico de Yucatán, Merida 97302, Mexico*

[4] *Coordinacion de la Investigación Científica, Universidad Nacional Autónoma de Mexico, Mexico City 04510, Mexico*

ABSTRACT

Results of a gravity survey of Socorro Island are used to investigate the volcanic structure of an oceanic island in the Mathematician Ridge, Eastern Pacific Ocean. The volcanic activity during the Quaternary is divided into pre-, syn-, and post-caldera stages, associated with a partly preserved caldera characterized by dominant alkali basalts and silicic peralkaline flows and domes. Recent Holocene activity includes basalt flows and cones of the Lomas Coloradas field. Bouguer anomalies correlate with the volcanic structure and topographic features, with low values over the summit caldera, intermediate-wavelength, intermediate-amplitude anomalies over the slope, and high-amplitude anomalies in the Lomas Coloradas. The regional anomaly field shows trends over the Ever-

*CORRESPONDING AUTHOR:
Jaime Urrutia-Fucugauchi, Programa Universitario de Perforaciones en Océanos y Continentes, Instituto de Geofísica, Universidad Nacional Autónoma de México, Mexico City 04510, Mexico; Instituto de Investigación y Estudios Avanzados Chicxulub, Parque Científico Tecnológico de Yucatán, Merida 97302, Mexico; Email: juf@igeofisica.unam.mx

ARTICLE INFO
Received: 18 November 2025 | Revised: 10 February 2026 | Accepted: 13 February 2026 | Published Online: 5 March 2026
DOI: https://doi.org/10.36956/eps.v5i1.2924

CITATION
Pavón-Moreno, J.A., Urrutia-Fucugauchi, J., Pérez-Cruz, L., et al., 2026. Unraveling the Volcanic Structure of Oceanic Islands—Gravity Survey of Socorro Island, Revillagigedo Archipelago, Mathematician Ridge, Pacific Plate. Earth and Planetary Science. 5(1): 1–19. DOI: https://doi.org/10.36956/eps.v5i1.2924

mann shield volcano, with broad positive anomalies over post-caldera deposits. The residual field shows small-wavelength anomalies over the caldera, caldera rim, slope, and pre- and post-caldera deposits, with isolated positive anomalies over pre-caldera volcanics and younger post-caldera deposits. Upward and downward analytical continuations, along with the first and second vertical derivatives, constrain the anomaly sources. Forward 2.5-D models with different geometries and density contrasts enable analysis of subsurface structure and stratigraphy. Basal sequences for the shield edifice are formed by basaltic and pyroclastic layered sequences. The residual gravity response is associated with units on top of the basal sequence and with post-caldera activity. From the gravity models, we estimate a post-caldera subsidence depth in the range of ~100 m that correlates with an estimated ~2 km^3 erupted volume and ~4.5 × 3.8 km caldera.

Keywords: Gravity Anomaly Models; Evermann Caldera Subsidence; Post-Caldera Volcanic Sequence; Eastern Pacific Ocean

1. Introduction

Geophysical methods have long been used to investigate the structure and stratigraphy of volcanoes and volcanic terrains[1–4]. Gravity modeling has been applied to investigate the structure and evolution of mid-ocean ridges, seamounts, and volcanic islands[5–9]. Here we present the results of a gravity survey of Socorro Island in the eastern Pacific Ocean (**Figure 1**). Socorro Island is characterized by the Evermann shield volcano and is the largest of a group of islands of the Revillagigedo Archipelago in the Eastern Pacific Ocean. The islands represent the emerged members of seamounts along the Mathematician Ridge at the Clipperton fracture zone[10,11].

Oceanic islands have been extensively studied to understand their formation and evolution within the oceanic crust, particularly in relation to plate tectonic processes such as mid-ocean ridge spreading, mantle plumes, and lithospheric structure[12]. These studies have led to the distinction between mid-ocean ridge basalts and ocean island basalts, which reflect contrasting magmatic sources and tectonic settings[13–15]. In this context, the Mathematician Ridge represents a short-lived and tectonically complex spreading system associated with plate reorganization in the eastern Pacific[10,11]. This geodynamic setting provides the framework for investigating Socorro Island, where gravity data can help constrain crustal structure, magmatic evolution, and the relationship between volcanic construction and tectonic processes.

The Socorro Island is characterized by silicic alkaline and peralkaline volcanism, which separates it from other islands in the Pacific Basin[16–18]. Sea floor spreading activity ended ~3.15 Ma ago, when activity shifted from the Mathematician ridge to the East Pacific Rise[11,19,20]. Volcanic activity in the Revillagigedo, formed by Clarion, Roca Partida, San Benedicto, and Socorro, has continued to the present, as evidenced by the basaltic eruptions in the southern sector of Socorro with the 1952–1953 Barcena eruption in San Benedicto, the 1993 submarine activity west of Socorro, and Evermann fumarolic activity[21–24].

Geophysical studies of Socorro and other islands in the Revillagigedo Islands are needed to understand the crustal structure, stratigraphy, and volcanic activity. Bohrson et al.[24] proposed the presence of a shallow magma chamber associated with the caldera, probably beneath the edifice or deeper in the upper oceanic crust. The Evermann prolonged activity with the pre- and post-caldera eruptions and spatial distribution of volcanic vents support a long-lived thermal anomaly and active magmatic plumbing system in Socorro.

Despite the evidence for long-lived magmatic activity and the proposed presence of a shallow magma reservoir beneath the Evermann caldera, the crustal structure and subsurface density distribution of Socorro Island remain poorly constrained. In particular, the geometry of caldera-related structures and the relationship between pre- and post-caldera volcanic units are still uncertain. In this study, we use gravity data to investigate the internal structure of Socorro Island, focusing on the Ever-

mann shield volcano and associated volcanic formations, with the aim of providing new constraints on the magmatic plumbing system and the volcanic evolution of this oceanic island (**Figure 2**).

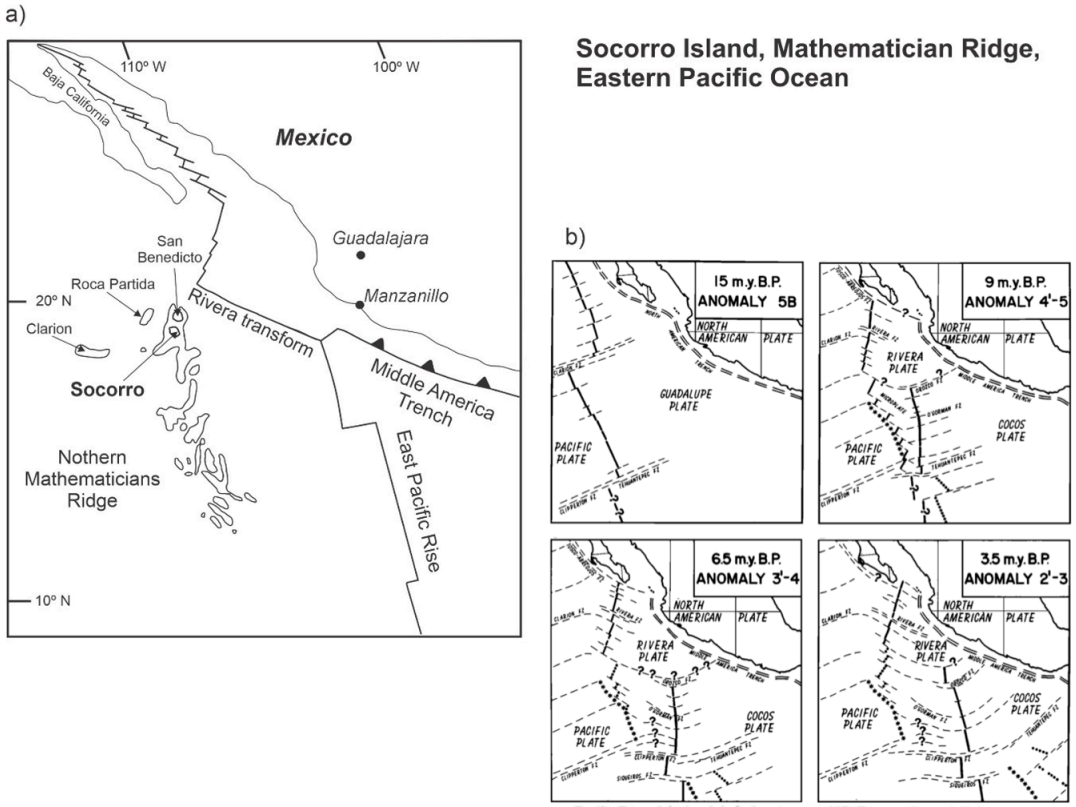

Figure 1. (**a**) Tectonic map of the central-eastern Pacific basin showing major tectonic elements of the East Pacific Rise, transform fracture zones, and the Middle America trench, and location of the Revillagigedo Archipelago formed by the Socorro, San Benedicto, Roca Partida, and Clarion Islands, part of a large group of seamounts in the northern Mathematician Ridge; (**b**) Schematic plate tectonic reconstructions for magnetic anomalies 5B, 4′–5, 3′–4, and 2′–3, showing the plate boundary reorganizations with fragmentation of the Guadalupe plate and formation of the Cocos and Rivera plates [10].

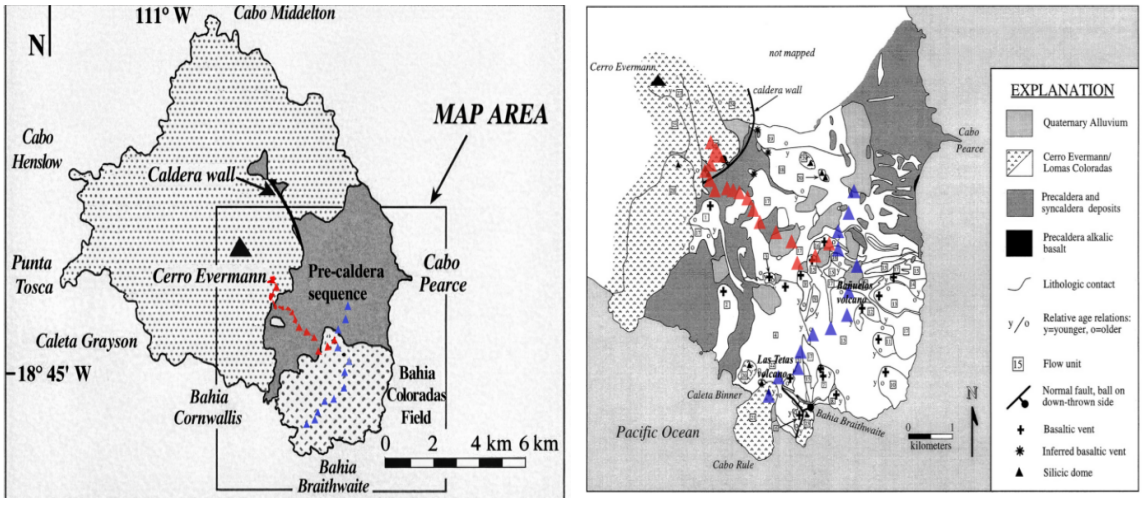

(**a**) (**b**)

Figure 2. (**a**) Schematic map of Socorro Island, showing the distribution of the pre-caldera units and the Evermann and Lomas Coloradas field. The area surveyed in the gravity study is located within the rectangle, forming the central-southern sector of the island; (**b**) Geologic map of the central-southern sector [24], indicating the location of gravity stations (see text for details).

2. Socorro Island

Seamounts and oceanic islands in the central–eastern Pacific record the interaction between seafloor spreading, intraplate volcanism, and plate reorganization processes [25]. The Mathematician Ridge and the Revillagigedo Islands are tectonically significant as they document the fragmentation of the Guadalupe Plate and the formation of the Cocos and Rivera plates during major plate reorganizations over the past ~25 Myr, recorded in bathymetric features and magnetic anomaly lineation patterns [10,11,16,17,20]. Plate reconstructions corresponding to magnetic anomalies 5B (~15 Myr), 4′–5 (~9 Myr), 3′–4 (~6.5 Myr), and 2′–3 (~3.5 Myr) are shown in **Figure 1b**. The latest reorganization, at about magnetic anomalies 2′–3, involved abandonment of the northern Mathematician Ridge as the Pacific–Cocos plate boundary, changes in relative plate motions, and the opening of the Gulf of California [10].

Within this tectonic framework, Socorro Island rises from the seafloor at some 3000 m depth [19,26]. The island exhibits an irregular elliptical morphology, with topography controlled by the subaerial exposure of the Evermann shield volcano, with a summit elevation of ~1120 m above sea level, and is characterized by a partly exposed caldera rim (**Figure 2**). Subaerial activity is characterized by alkaline and peralkaline magmas and marked by pre-, syn-, and post-caldera major phases. In the central-southern sector, post-caldera activity includes the Lomas Coloradas field, composed of basaltic lava flows and cinder cones with associated lava and spatter flows (**Figure 2**). The study area is located in the central-southeastern sector of the island, from the summit caldera sector to the coastline. In this area, it is possible to investigate the volcanic structures and stratigraphic units associated with the pre-, syn-, and post-caldera eruption phases, as well as the development of the Lomas Coloradas activity. The Navy Station, located in the southeastern sector of the island, provides support and logistics for the study.

Geologic mapping has been reported for the central-southern portions of the island [16,24]. The studies, combined with geochemistry and radiometric dating, have documented the activity buildup, with the changing patterns of magmatic activity from dominantly explosive to effusive, leading to the formation of a caldera and post-caldera volcanism [16,18,24]. Bohrson et al. [24] proposed that a change in magma degassing is associated with the caldera formation, marking the change in the character of the activity. Calderas occur in different tectonic settings and are characterized by a wide range of sizes, magma compositions, and eruptive histories. Calderas can form by the collapse/subsidence of volcanic structures above magma chambers during or after large eruption episodes. Their studies have attracted considerable interest, and in the past decades, a combination of field-based geological, geochemical, and geophysical surveys and analogue and theoretical modeling has contributed to the understanding of calderas and caldera-forming mechanisms [27,28]. At the same time, major questions still remain, with some caldera types and volcanic environments remaining less well investigated.

Peralkaline calderas appear related to high extension rates, like the East African rift, some convergent margins (e.g., New Zealand), and intra-plate volcanic islands (e.g., Canary Islands) [29,30]. Volcanic environments with low magma production rates require relatively long repose periods with magma stored in shallow chambers [27,31]. The end of active rifting in the Mathematician Ridge, with a jump in seafloor spreading to a new location in the East Pacific Rise, occurred ~3.15 Myr ago [10,11], raising questions about volcanic activity, particularly the thermal anomaly, magma supply rates, and caldera formation in Socorro Island.

The eruptive history of subaerial activity has been documented from Ar/Ar dating [24]. Dates on peralkaline rhyolites and trachytes range from ~540 to 370 kyr, documenting several explosive eruption episodes with intervening repose periods of ~30 kyr. Dates on post-caldera flows are around 182 to 15 kyr; with an intra-caldera rhyolite dome and rhyolite flows southeast of the caldera wall giving dates of around 150 and 152 kyr, respectively. The caldera-forming eruption likely occurred at ~370 kyr, contemporaneous with the emplacement of rhyolitic ash-flow tuffs. This event was followed by a prolonged period with no recorded major explosive events, prior to the onset of post-caldera volcanic activity. If the

caldera formed at a later time (i.e., before ~180 kyr), it may have involved magma withdrawal or migration at depth, resulting in caldera collapse [24]. The caldera rim is partly exposed as an arcuate topographic feature. Inside the caldera wall, there are lava flows of Cerro Evermann, silicic domes, and alluvium-fill deposits. On the flank, outcrops of pre- and syn-caldera deposits extend towards the shoreline. Close to the caldera wall, there are several inferred basaltic vents.

Post-caldera activity is predominantly represented by silicic peralkaline flows and domes of Cerro Evermann, and by lava flows and cinder cones of Lomas Coloradas, which also includes some trachyte domes near the coastline. Radiometric dates for basalt flows range between 150 and 70 kyr, documenting contemporaneous eruptions of silicic and basaltic magmas in Socorro [24]. Farmer et al. [23] reported radiocarbon dates for lacustrine deposits of about 4690 and 5040 yr BP within the Lomas Coloradas volcanic sequence. These dates provide evidence for Holocene activity with alkalic basalt eruptions from low-elevation fissures and cones in the southeastern sector. The geologic mapping by Bryan [16] and Bohrson et al. [24] identifies several flow units (marked by numbers) and several young basaltic vents, which cover the pre- and syn-caldera deposits. Outcrops of these deposits are mapped on the southwestern and northeastern sectors, with smaller outcrops in the central zone (**Figure 2b**).

Geophysical surveys of Socorro Island have been reported, providing constraints on the regional structure and volcanic activity. They include aeromagnetic, gravity, gamma ray, and paleomagnetic studies [32–36]. Paoletti et al. [35] interpreted a magnetic low in the central sector in terms of a hot, deep magma body, some 5 km below sea level. The aeromagnetic anomalies were interpreted in terms of a nested caldera structure. Tapia et al. [36] focused on the extensional systems and caldera structure, marked by semi-circular regional gravity and magnetic anomalies, supporting the presence of a thermal anomaly associated with a deep magma reservoir.

3. Materials and Methods

The gravity survey was conducted along two sectors crossing the summit caldera area, the slope, and the zone of Lomas Coloradas (**Figure 3**). We used a LaCoste & Romberg model-G gravity meter for the survey, with a tie station located at the Navy Base Camp. The locations of the stations were determined using a Garmin GPS meter. The altitude was estimated from the GPS measurements, complemented with the (National Institute of Geography) INEGI topographic database and calibration at the tie station. The geologic map of the southeastern sector by Bohrson et al. [24] provides a reference to the volcanic structures and stratigraphy (**Figure 3b**).

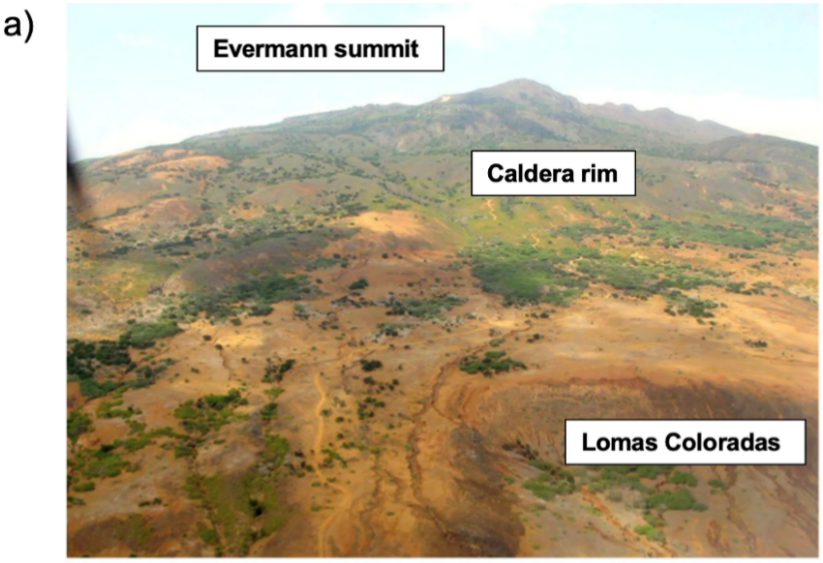

Figure 3. *Cont.*

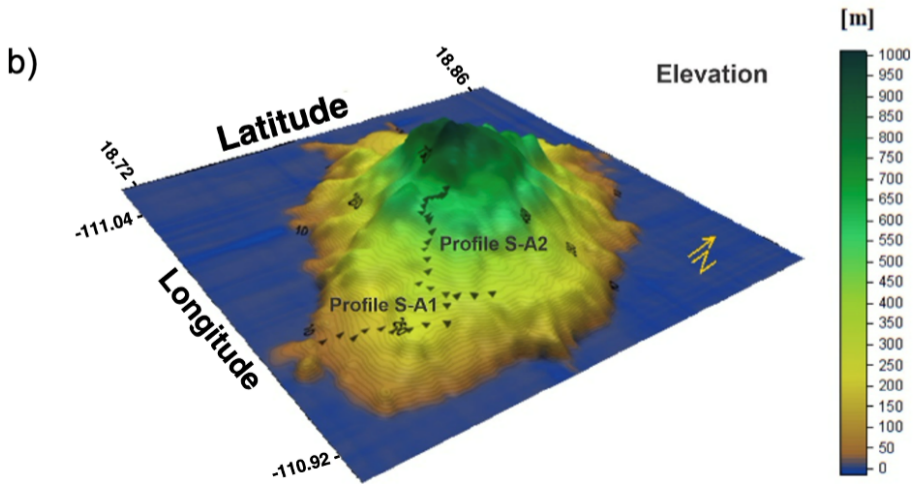

Figure 3. (**a**) Socorro Island, Revillagigedo Archipelago, view from the southeast toward Evermann volcano. The Lomas Coloradas volcanic field is highlighted in red, while the summit and the caldera rim are visible in the background; (**b**) Three-dimensional oblique topographic view of Socorro Island showing the location of the gravity profiles surveyed. Colored triangles indicate individual gravity stations along profiles S-A1 and S-A2, which cross key volcanic features including the caldera rim and volcanic flanks.

The gravity stations are distributed following the topographic relief, along paths rather than forming straight lines. Profile S-A1 is about 6 km long, crossing the slope, pre-caldera deposits, and the Lomas Coloradas field. It includes 13 stations distributed at approximately 500 m intervals. Profile S-A2 is about 5 km long, crossing the caldera deposits, caldera rim, and slope with syn- and post-caldera units. The survey includes 18 gravity stations with spacing ranging from 200 m to 500 m, following local topography, conditions, and accessibility constraints, which preclude the acquisition of uniformly spaced measurements.

The gravity readings were reduced to calculate the Free Air and Bouguer gravity anomalies [37,38]. A standard density of 2.67 g/cc was used to determine the Bouguer anomalies [39]. There are no stations of the gravity network in the Revillagigedo Islands, and a temporary station was established and occupied for the subsequent survey campaigns. Reference to the gravity network in the mainland is planned as part of the reference network gravity program [40].

4. Results

The Bouguer gravity anomalies fall in the range between −3 mGals and 25 mGals. The range is characteristic of oceanic islands, in contrast to the large negative Bouguer gravity anomalies over continental areas and volcanic arcs [41].

Profile S-A1 (oriented NE–SW) shows two broad anomalies over the northeastern sector of the pre-caldera and post-caldera deposits and over the Lomas Coloradas field. Anomaly along profile S-A2 (oriented NW–SE) shows a correlation with the structure, with an anomaly corresponding to the caldera rim and short wavelength anomalies along the flank over the pre-caldera and post-caldera deposits.

The regional anomaly field estimated using second- and third-degree polynomial fits gave similar results, with anomaly trends and a broad positive anomaly over the Lomas Coloradas (**Figure 4**). The corresponding residual fields after subtracting the regional polynomial fields show smaller wavelength anomalies over the caldera, slope, pre- and post-caldera deposits (**Figure 4c**). The residual field shows a positive well-defined anomaly in the northeastern sector of the pre-caldera deposits and smaller amplitude isolated anomalies over the Lomas Coloradas. These anomaly patterns correlate with results from the upward and downward analytical continuations and first and second vertical derivatives, providing insight for qualitative analysis of anomaly sources (**Figure 5**). Upward continuation up to 500 m reference level (**Figure 5a**) delineates a trend over the caldera rim and slope, a broad maximum at the south-

eastern sector, and a small amplitude high in the northeastern sector of pre-caldera deposits. Downward continuation down to 100 m (**Figure 5b**) and 200 m (**Figure 5c**) reference levels delineates the anomaly over the caldera deposits and rim, and three maxima over the post- and pre-caldera deposits. Downward continuation to the 200 m level separates the three maxima, isolating the anomaly over the northeastern sector of pre-caldera deposits. The downward-continuing field correlates with the first vertical derivative field, constraining the relative depths of anomaly sources from gradient analysis.

Samples from outcrops were collected along transects at 24 sites. Bulk density was determined using the fluid immersion method, with three representative samples analyzed at each sampling site. Measured densities range from 1.7 to 3.02 g/cc. Samples were grouped into four categories based on their geographic location and lithology. Mean density values for each group are 2.38, 2.47, 2.70, and 2.80 g/cc, respectively (**Table 1**).

For the analysis and contour visualization, data were interpolated into a regular grid using inverse distance weighting and kriging and contoured with Surfer. To further evaluate the interpolation methods, the elevation data were interpolated and compared with the digital terrain map [42]. Both methods reproduce the main topographic patterns, with kriging yielding smoother contours; therefore, gravity anomaly maps were constructed using the kriging method. The Bouguer gravity anomaly maps display spatial variations in amplitude and wavelength across the study area (**Figure 4**). Lower anomaly values are observed in the central part of the island, whereas intermediate values occur toward the slopes, and higher anomaly amplitudes are observed in the southern sector. In the northeastern sector, a localized gravity high with amplitude comparable to that observed in the southern sector is identified (**Figure 4a**). To separate long- and short-wavelength components, the data were processed using second and third-degree regional polynomial fitting, first and second vertical derivatives, and upward and downward analytical continuations [43–47]. Upward continuations were calculated for reference levels of 0.5 and 1.0 km. Downward continuations were calculated for reference levels of 0.1 and 0.2 km.

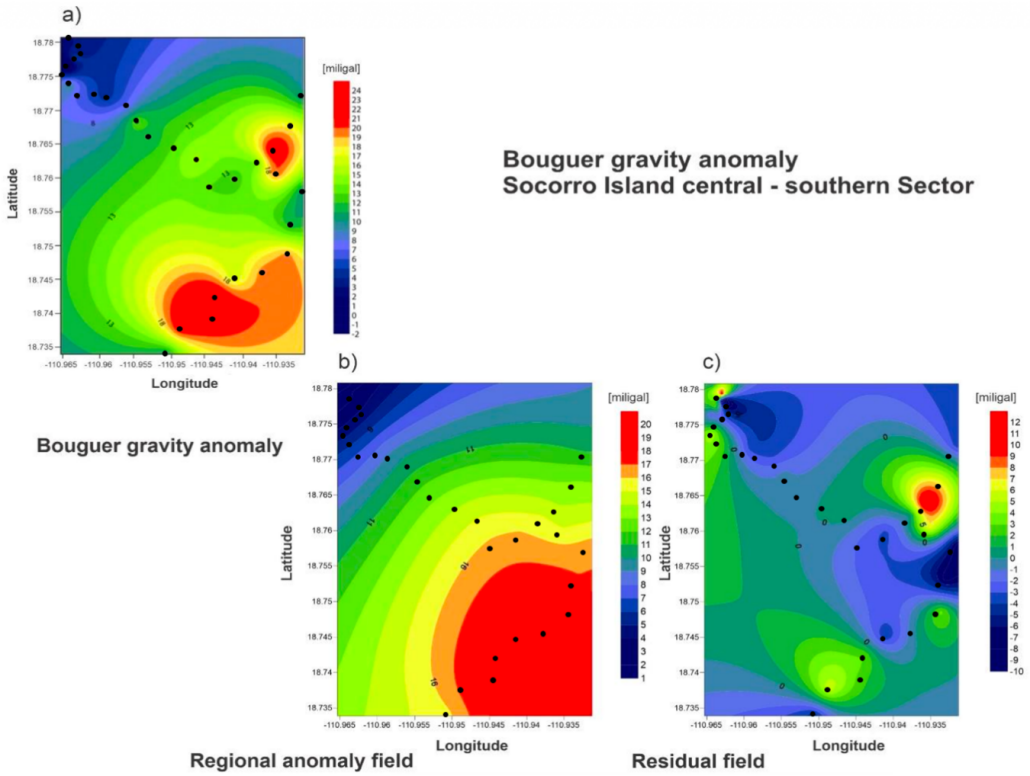

Figure 4. (**a**) Bouguer gravity anomaly of the central-southern sector of Socorro Island; (**b**) Regional gravity field for third-degree polynomial; (**c**) Residual anomaly field after subtraction of third-degree polynomial.

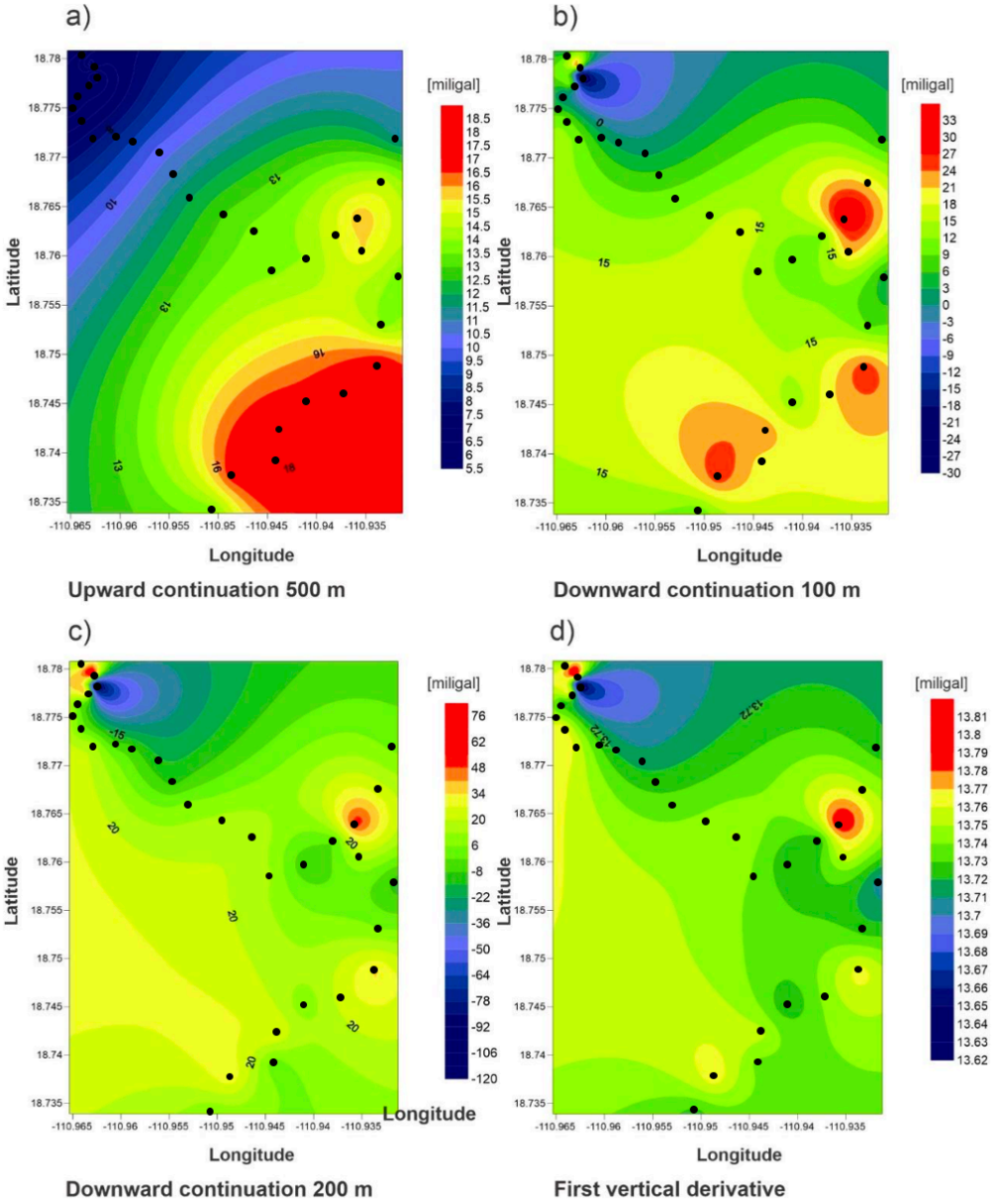

Figure 5. Analytical continuations of the gravity field. (**a**) Upward continuation to 500 m; (**b**) Downward continuation to 100 m; (**c**) Downward analytical continuation of the gravity field to 200 m; (**d**) First vertical derivative of the gravity field.

Table 1. Summary of rock density measurements by lithologic group and sampling location.

Group	Number of Samples	Location	Lithology	Mean Density (g/cc)	Std. Dev. (g/cc)
1	9	Evermann Caldera Rim	Basalts	2.80	0.55
2	6	Pre-caldera deposits	Peralkaline trachytes and rhyolites	2.47	0.41
3	3	Bañuelos Volcano	Basalts	2.70	1.40
4	6	Lomas Coloradas	Vesicular basalts	2.38	0.20

5. Forward Modeling

The shallow structure and stratigraphy are further analyzed using forward 2.5-dimensional (2.5-D) polygonal models[47–50]. Calculation of synthetic anomalies was made using the WinGlink geophysical software. The residual field after subtraction of the regional field is used for forward modeling. Different geometries and density contrasts were examined, and synthetic anomalies were fitted to observed anomalies.

There are no drilling and log data, and model parameters are defined by fitting the calculated and observed anomalies [43,45,47]. Initial model parameters were constrained from the geological studies [18,24] and qualitative analysis of the Bouguer anomalies, regional-residual fields, upward and downward analytical continuations, and first vertical derivative calculations.

The gravity models were determined considering density values constrained by the range of densities from surface rock samples. Groups 1 to 3 (**Table 1**) show consistent density values, suggesting comparatively homogeneous conditions at the scale sampled. In contrast, the relatively high-density variability observed in Group 4 likely reflects the combined effects of a limited number of samples and significant lithological and textural heterogeneity, particularly related to variable vesicularity and alteration within basaltic units. It is suggested that, while surface-derived rock density measurements may not fully represent subsurface volumes due to scale-dependent heterogeneity [51–53], adequate spatial and lithological sampling can nevertheless provide robust first-order constraints for gravimetric model parameterization [54]. Accordingly, the densities adopted in the models fall within the variability observed in the measured dataset, rather than relying on fixed mean values for each lithological group, and are intended to represent effective bulk densities at the scale of the gravity data. Under these assumptions, the resulting models provide a consistent first-order fit to the observed gravity anomalies, supporting the use of the selected density range for the subsurface density structure.

Models for profiles S-A1 and S-A2 explore different arrangements of subsurface bodies associated with the volcanic features and pattern of gravity anomalies (**Figure 6**). Profile S-A1 shows a broad positive 5 mGal anomaly over the Lomas Coloradas volcanic field and a smaller amplitude anomaly over the post-caldera units in the northern part of the profile. Profile S-A2 shows a minimum on the summit caldera depression, a ~4 mGal high on the caldera rim, followed by a minimum on the outer caldera side on top of pre-caldera deposits. On top of the post-caldera sequences, there is a series of small amplitude, large wavelength positive and negative anomalies. The larger amplitude anomaly ~7 mGals is in the southeastern area over post-caldera deposits north of the Lomas Coloradas. The different sets of models assume lateral contrasts with distinct large bodies as sources of the positive anomalies on top of the pre-caldera sequence. The basal layer is assumed to form the volcano structure. Depths to the top of this layer range from ~200 m to ~500 m below sea level, with most models around 200–300 m below sea level. The top of this layer was kept with low relief, although models with abrupt relief were also tested.

Polygonal models (PM) are calculated to analyze the structure and stratigraphy. The results for two sets of models are presented (**Figure 6**). PM4-5 type models incorporate 4- or 5-polygonal bodies (layers). For profile S-A1, a large body (black; 1.4 g/cc) sits beneath the Lomas Coloradas field with a lateral contrast to the pre- and post-caldera sequences (light gray and cross-hatched; 0.92 and 1.6 g/cc) in the northern sector of the profile (**Figure 6a**). For profile S-A2, a large body accounts for the caldera wall deep structure (black), and two bodies (cross-hatched) account for the anomalies on the flank over the post-caldera sequences (**Figure 6b**). Other model types evaluated incorporate an additional number of polygonal bodies and a layered basal sequence that results in slightly thinner shallow bodies. Examples of PM-7 type models are shown in **Figure 7**. Models for profile S-A1 show a similar body (black) beneath the Lomas Coloradas field; bodies for the northern part of the profile can be represented by different geometries assuming vertical density contrasts (light-gray units), which appear more consistent with the geological considerations (**Figure 7a**). Models keep the basal sequence tilting towards the coastline with smooth relief, in contrast to the other set of models (**Figure 6**). Models for profile S-A2 are modeled with shallow bodies (light-gray units) with larger lateral extent (**Figure 7b**). The basal sequence is formed by layers that tilt following the slope of the volcanic structure. The caldera depression is modeled assuming a shallow depression. The caldera rim is modeled by a body representing the structural wall. The anomalies on the flank are modeled by shallow bodies (**Figure 6**).

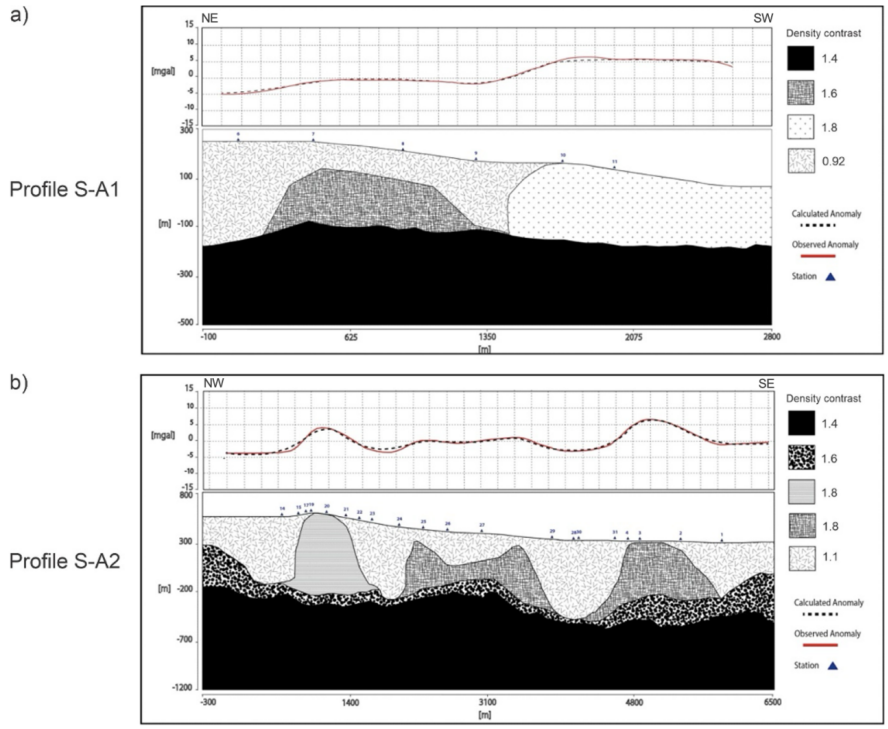

Figure 6. Geophysical 2.5-D models for profiles S-A1 and S-A2. These models incorporate 4–5 layers; density contrasts are indicated for the units. (**a**) Profile for the pre- and post-caldera deposits; (**b**) Profile for the caldera, rim, and slope. The observed and synthetic gravity anomalies are indicated by the blue and red curves, respectively (see text for discussion).

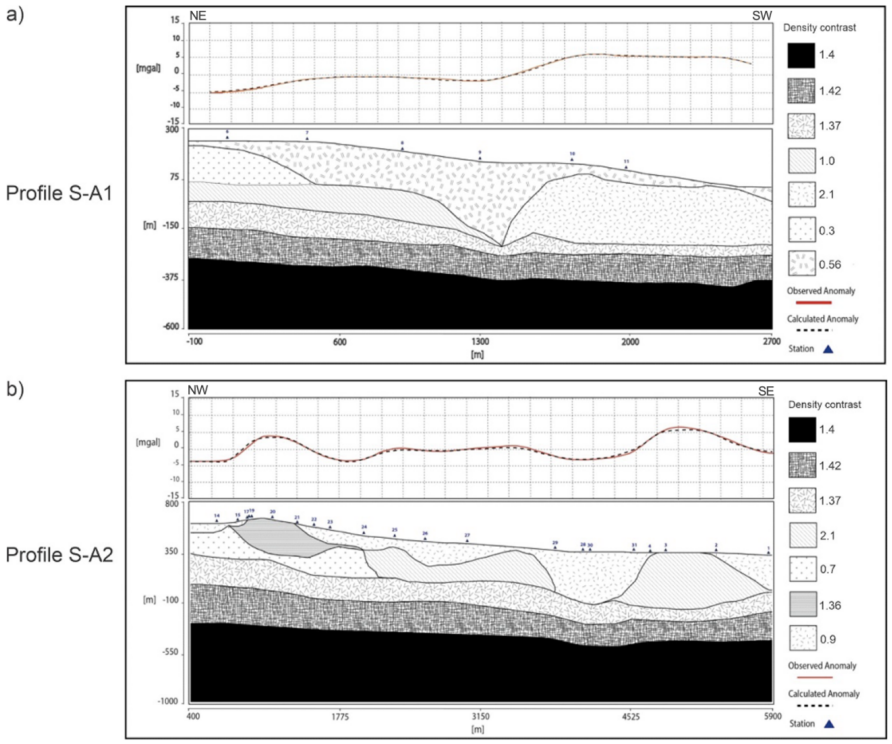

Figure 7. Geophysical 2.5-D models for profiles S-A1 and S-A2. These models incorporate 7 layers; density contrasts are indicated for the units. (**a**) Profile for the pre- and post-caldera deposits; (**b**) Profile for the caldera, caldera rim, and slope. The observed and synthetic gravity anomalies are indicated by the blue and red curves, respectively.

Models for profile S-A1 over Lomas Coloradas show a pre-caldera sequence covered by post-caldera flows (**Figures 6a and 7a**). PM-7 models are preferred because they keep the basal layers with a regional tilt towards the coastline. Thickness and depth to the top of the source bodies depend on the density contrasts and on the number of bodies incorporated. The source bodies account for the isolated anomalies over the northeastern sector beneath the Bañuelos volcano and the Lomas Coloradas cinder cone field (**Figure 2b**). Source bodies require further constraints and appear located on the thick southward-dipping sequence of the shield volcano.

Models for profile S-A2 assume a local basement formed by the units constituting the shield volcano, with bodies associated with the volcanic units on top (**Figures 6b and 7b**). PM-7 models incorporate the basal layers with flat relief and regional tilt that follow the volcano's structure. The models for the caldera depression, rim, and slope consider source bodies of different geometries and density contrasts. The residual gravity anomaly shows a low over the caldera depression, followed by a high over the caldera rim. This is followed by a series of maxima and minima over the flank. In the area covered by the pre-caldera deposits and post-caldera flows, residual anomalies show a broad minimum and a larger amplitude maximum.

6. Discussion

Socorro Island is formed by volcanic activity, with a shield volcano constructed on the ocean floor in the northern sector of the Mathematician ridge. Bathymetry in this area of the Revillagigedo Archipelago is shallower, associated with the ridge and the Rivera and Clarion fracture zones, and characterized by numerous seamounts (**Figure 1**). The island subaerial topography is dominated by the Evermann structure, and the post-caldera deposits (**Figures 2** and **3**). Post-caldera activity includes dominantly silicic peralkaline lava flows and domes, and some alkali basalt flows and cones inside the caldera and slope. The Lomas Coloradas in the southeastern sector includes dominantly alkaline basalt flows and cones. Volcanological studies and geological mapping have raised questions related to the structure of the volcanic edifice, subsurface stratigraphy, characteristics of the magma reservoir inferred at relatively shallow depths beneath the caldera and the associated plumbing system, and structures related to the Holocene volcanism [16,18,24].

Our gravity survey conducted over the eastern area of Socorro Island was directed to explore the shallow crustal structure and volcanic stratigraphy [24,33]. The Bouguer gravity anomaly and regional and residual fields correlate with the volcanic topography. The regional field shows a gravity low over the caldera summit and rim, a gravity trend over the slope, and a broad high over the Lomas Coloradas field. The residual anomaly shows several isolated highs and lows that correlate with surface features, with three maxima over the Las Tetas and Bañuelos volcanoes, and groups of cinder cones (**Figure 2b**). The caldera area is marked by a gravity low and a high, characterizing the summit caldera depression and wall structure.

The Bouguer anomaly shows caldera depression marked by a −2 mGal negative anomaly, interpreted as resulting primarily from low-density alluvial-fill and pyroclastic deposits infilling the caldera. The caldera wall is marked by a 5 mGal high anomaly, which appears to be associated with a deep structural feature. The depth of the caldera depression in the forward models depends on the geometry of subsurface layers and density contrasts. The caldera structure and the extent of collapse are related to eruptive dynamics and the erupted magma volume [27]. Models incorporating a large caldera wall structure result in large depth estimates for collapse or subsidence (**Figure 6**). The Model assumes that the central portion of the volcanic structure was affected by faulting. The caldera wall is only exposed in the southern sector; in the northern part, it might be affected by faulting and buried by lava flows (**Figure 2**). However, no evidence for a fault has been documented in the geologic mapping studies [24]. Models assuming a caldera wall not affected by significant faulting show caldera depression depths of around 100 m.

Complex caldera structures show collapse depressions, some associated with nested structures formed by multiple explosive episodes [27,28,53]. In silicic peralkaline complexes, nested calderas have been recog-

nized[54]. In Socorro, tuff units in the stratigraphic column document explosive events that might have resulted from caldera-forming events. The shape and size of the caldera are inferred from the partial rim exposures and topography. Bohrson et al.[24] reconstructed an elongated caldera structure with a NW–SE orientation, some 4.5 × 3.8 km in size, which is comparable to other peralkaline calderas[54]. Acocella[28] reviewed the relations between caldera diameter and subsidence (**Figure 8**). For caldera diameters of around ~4 km, the depth of subsidence varies up to a few hundred meters, depending on the erupted volume of magma and evolutionary stage. Stage 4 calderas are associated with large magma volumes, whereas stage 2 calderas usually involve small volumes. Bohrson et al.[24] estimated a minimum volume for the caldera, in the order of 2 km^3 (dense rock equivalent). This will place the caldera within the range of a few hundred meters of subsidence, compatible with depth estimates of around ~100 m as in PM-7 type models (**Figure 7**). Bohrson et al.[24] remarked that the erupted volume might be larger, with possible nearby ocean deposits and/or buried by younger units. The uncertainties emphasize the need for further geophysical data on subsurface stratigraphy.

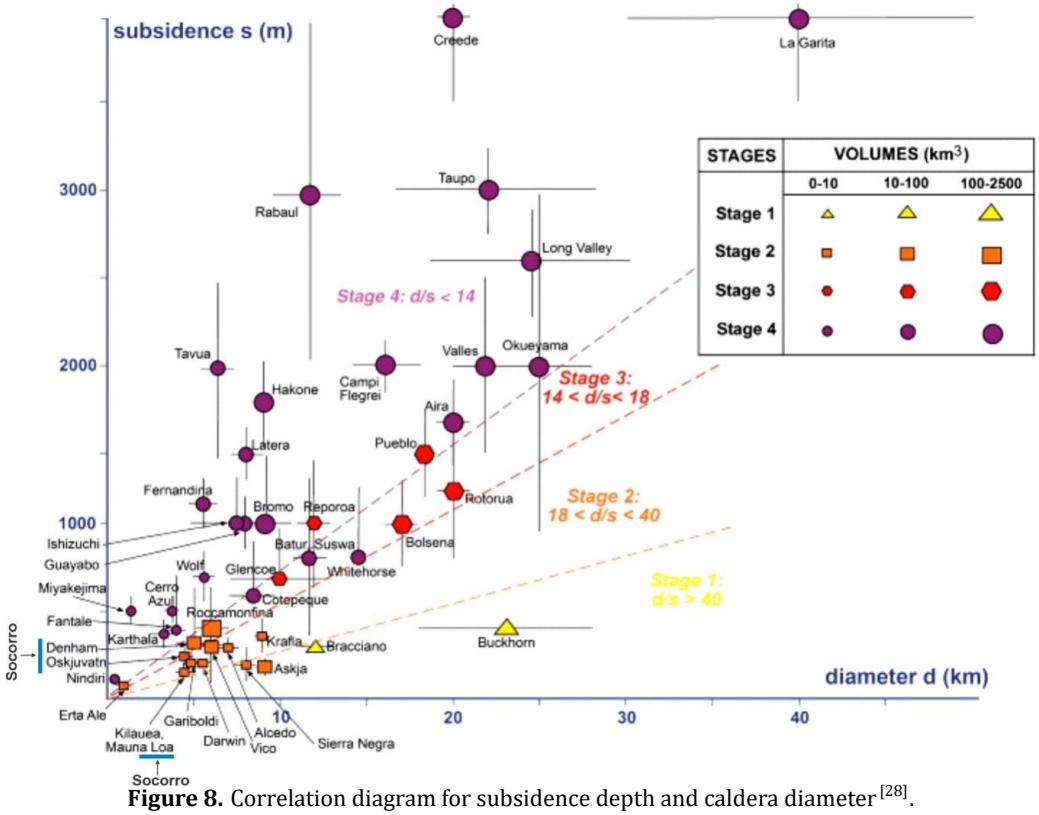

Figure 8. Correlation diagram for subsidence depth and caldera diameter[28].

Note: The symbols represent different evolutionary stages (see text). For caldera diameters of around ~4 km, the depth of subsidence varies up to a few hundred meters, depending on the erupted volume of magma and evolutionary stage. In the case of the Evermann caldera, Bohrson et al.[24] estimated a minimum volume in the order of 2 km^3, which places the caldera within the range of a few hundred meters of subsidence (indicated by the arrows), compatible with depth estimates from the gravity models of around ~100 m.

The estimates for erupted volume and subsidence depth for Socorro are comparable to peralkaline calderas, with intermediate diameters of less than 12 km and subsidence depths of <300 m[27,55,56]. The caldera wall heights range from a few tens to hundreds of meters; for example, the Pantelleria caldera has a wall height of about 90 m, with an estimated erupted volume of 7 km^3. The calderas in the Canary Islands are an exception, with much larger sizes, erupted volumes, and subsidence depths likely representing complex calderas constructed by multiple eruption episodes[27,29]. The regional models for the entire volcanic edifice consider a shield-like structure similar to basaltic volcanoes in Hawaii. Models for Hawaiian shield volcanoes incorporate shallow magma chambers, with caldera formation due to magma withdrawal and extension related to the

magma intrusions and surface collapse [27,57]. The models with small collapse depths and reduced summit collapse zones may be more representative of Socorro Island (**Figure 8**). The model incorporates asymmetric collapse and sill intrusions resulting in flank eruptions, which may also be related to faulting and extension of the shield. Post-caldera magma intrusion into the central zone above the magma chamber may result in uplift and resurgence (e.g., Pantelleria caldera [54], which accounts for the Evermann summit. The magma intrusion is responsible for the prolonged volcanic activity registered in the southeastern island sector.

The broad positive anomaly over the Lomas Coloradas corresponds to a 2 × 1.5 km zone with monogenetic cones and lava flows [24]. The ~12 mGal maximum in the northeastern sector corresponds to the Bañuelos cone, over a 0.5 × 0.25 km zone (**Figure 2b, 4a,** and **5b**). The broad anomaly over Lomas Coloradas separates into smaller wavelength isolated anomalies in the first vertical derivative and downward continuation maps. Downward continuation to 100 m shows two positive anomalies, corresponding to volcanic features (**Figure 7**). The southern anomaly corresponds to Las Tetas volcano, and the southeastern one is over a group of small cinder cones. Correlation of the patterns in the downward-continued fields provides insight into the relative depths of the source bodies (e.g., **Figure 5**). The upward and downward continuations, and the first vertical derivative anomaly maps, delineate the response associated with the caldera depression and rim.

Paralkaline calderas are usually shield-like, similar to explosive basaltic calderas [27,55,56]. Calderas forming on oceanic island shield volcanoes develop through stages of collapse and filling. Walker [57] proposed that intruding magma produces shield expansion with surface extension and collapse, which, along with magma withdrawal, results in caldera formation. The morphology can be modified by resurgent activity and post-caldera deformation. Size and morphology of calderas are highly variable depending on eruption style, magma composition, eruptive history, collapse mechanism, and post-caldera activity [27]. Acocella [28] identified four stages of caldera development from analogue modeling and field observations, characterized by (stage 1) downsag, (stage 2) reverse ring fault, (stage 3) peripheral downsag, and (stage 4) peripheral normal ring fault. Acocella [28] proposed that the caldera diameter/subsidence ratio relates to the evolutionary stage (**Figure 9**). For caldera diameters of around ~4 km, the depth of subsidence varies up to a few hundred meters, depending on the erupted volume of magma and evolutionary stage. In the case of the Evermann caldera, Bohrson et al. [24] estimated a minimum volume in the order of 2 km^3, which places the caldera within the range of a few hundred meters of subsidence (indicated by the arrows in the diagram), compatible with the depth estimates from the gravity models of around ~100 m.

Data on stratigraphy and thickness of the volcanic sequences have been used to estimate eruption volumes and rates [24]. Subaerial pre-and syn-caldera rates are in the order of ~1–5 10^{-5} km^3/yr, which are in the range of those documented for mantle plume oceanic islands. On the other hand, minimum growth rates for Socorro of about > 7 × 10^{-5} km^3/yr are much higher than growth rates for non-hotspot volcanoes in the Pacific. The erupted volumes and growth rates relate to volcanic evolution and mantle source [17,25,27,58,59].

Forward models with contrasting geometries and density contrasts are tested. Models in **Figures 6** and **7** show the structures that fit the observed anomalies and geological considerations. Models show distinct structures for the shallow volcanic units, which can be evaluated with additional modeling and drilling data. The results show non-uniqueness in the solutions for potential field models. The end models that fit the observed anomalies show the effect of considering four and seven source units for the analysis. The inclusion of source bodies is reflected in the shallow structure in the caldera rim zone and slope. This is associated with possible undetected units and internal density variations resulting from changes in fracture density or porosity. Generally, the effects of the non-uniqueness in potential field modeling increase with the sought- after special resolution. Modeling can be further evaluated by drilling and studies with additional techniques.

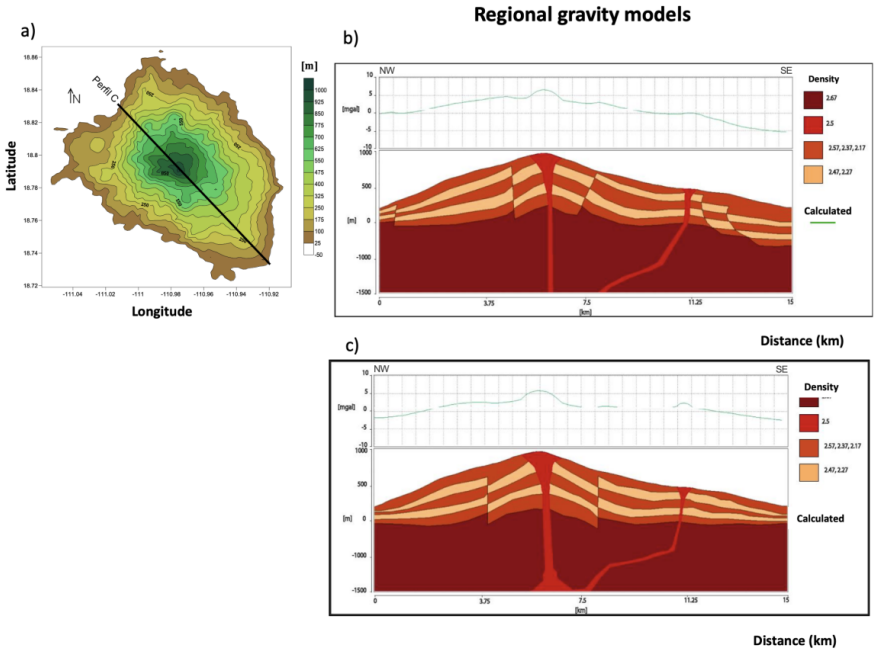

Figure 9. Regional gravity models for Socorro Island. (**a**) Location of profile crossing the central zone and the Evermann volcano. Gravity anomaly models with (**b**) and without (**c**) faults in the southeastern sector, both including dike intrusions in the volcanic edifice (see text for discussion).

Based on analysis of the upward and downward analytical continuations, the first and second vertical derivatives, and regional-residual separation, the source bodies of the residual anomalies correspond to shallow contrasts. Shallow anomaly sources correlate with the surface geological observations. Initial geometries in the modeling were constructed from qualitative assessments of geologic data and regional and residual fields, analytical continuation fields, and gradient maps. The downward range of flow units of the Cerro Evermann, reaching the coast, may represent analogs of the older pre-caldera sequence. The basal sequence may be modeled by a single thick unit of uniform density. Alternatively, it may be formed by basaltic lava flows and pyroclastic units, which result in layered sequences with vertical density contrasts. Different geometries were considered for the basal sequence. Topographic relief for the top surface of these basal units may contribute to the gravity anomalies. Alternatively, the gravity response may be due to units on top of the basal sequence, associated with the underground conduit system in Lomas Coloradas. Other differences among the models are reflected in the thickness of the units, with thicker units in PM-4-5-type models compared to thinner units in PM-7-type models (**Figures 6** and **7**).

The regional structure of the volcanic island has been examined using modeling of satellite and airborne magnetic and gamma-ray survey data [35,36]. The regional pattern shows curved semicircular anomalies that constrain a large caldera complex. The magnetic anomaly shows a central minimum, associated with a hot magma body lying at depth in the crust, estimated at around 5 km b.s.l. [35]. To further analyze the volcanic structure in the central zone, models are calculated for a regional profile crossing the central zone. The models allow examining the stress field, post-caldera activity, underground conduit system, dike intrusions, and faulting of the edifice [59,60]. The profile crosses above the Evermann caldera (**Figure 9a**). It is about 15 km long and oriented NW–SE. The topography of the volcanic edifice is steep on its NW side as compared to that on the SE side, which is also mirrored in the bathymetry with low-angle slopes in the southeastern sector [11]. The Bouguer gravity anomaly for the central-southern sector of the island shows a regional anomaly trend that correlates with the topography of the volcanic edifice, with anomalies over the caldera and the post-caldera Lomas Coloradas. Different geometries and density contrasts are used in the

models, which incorporate major structural elements of the shield volcano, including a shallow magma chamber and a volcanic conduit system associated with post-caldera activity. Two models are included in **Figure 9b,c** that show the volcanic edifice structure, radial and circumferential fracture patterns, magma conduit system, sills, and faulting. The caldera rim is exposed on the southeastern side. It is buried or not preserved on the northwestern side, which is associated with a regional fault. In the models, the occurrence of dikes, faults, and shallow magmatic activity in the Lomas Coloradas volcanic field was analyzed.

Recent studies in the Clipperton-Clarion zone in the Central Eastern Pacific have been investigating the extensive deposits of sulphides and polymetallic nodules, with deep-sea mining exploration projects [61–64]. The abyssal plain at depths around 4–5 km is characterized by a unique biodiversity with organisms adapted to the deep cold conditions [63,64]. The polymetallic nodules are rich in nickel, cobalt, copper, manganese, and zinc, with mineral contents of interest for mining activities. The zone has been relatively unexplored, including studies of the oceanic crustal structure, age, magnetic anomalies, faulting, and volcanic features [65]. This is partly due to the challenges of marine geophysical projects and the logistical and technological requirements.

7. Conclusions

The Bouguer gravity anomaly shows a gravity low over the Evermann caldera with intermediate wavelength and amplitude trends over the slope and high amplitude anomalies in the Lomas Coloradas field. The residual field reveals positive anomalies in the northeastern sector of the pre-caldera deposits and small-amplitude isolated anomalies over the Lomas Coloradas field. The anomalies are followed in the upward and downward analytical continuations and in the first and second vertical derivatives, which constrain the depths and shapes of the anomaly sources. Forward 2.5-D models enable analysis of volcanic structure and stratigraphy. The basal sequence can be modelled as a single, thick unit of uniform density, or alternatively as a basaltic and pyroclastic layered sequence with vertical density contrasts. Gravity response may be due to units on top of the basal sequence, associated with the conduit system for post-caldera and Lomas Coloradas activity.

The gravity models provide constraints on post-caldera volcanic activity. The positive anomaly over the Lomas Coloradas delineates a zone measuring 2 × 1.5 km, characterized by monogenetic cones and lava flows. The small maximum in the northeastern sector corresponds to the Bañuelos cone, over a 0.5 × 0.25 km zone. The broad anomaly over Lomas Coloradas separates into small-wavelength isolated anomalies in the first vertical derivative and downward continuation maps. Pattern correlation in the downward-continued fields constrains the relative depths of the source bodies. Downward continuations to 100 m and 200 m show two positive anomalies, corresponding to volcanic features. The southern anomaly corresponds to the Las Tetas volcano, and the southeastern one is over a group of small cinder cones.

The caldera depression is marked by a −2 mGal low, and the caldera wall by a 5 mGal high associated with deep structures. Depth estimates of caldera depression depend on subsurface geometry and density contrasts that record collapse related to eruptive dynamics and magma volume. Models incorporating a large caldera wall yield large collapse depth estimates. The caldera wall is exposed in the southern sector; in the northern sector, it might be affected by faulting and/or buried by lava flows. Preferred models show subsidence depths of around 100 m. Shallow estimated depths for subsidence appear compatible with an erupted volume of around 2 km^3 and an estimated size of 4.5 × 3.8 km for the caldera, within the ranges documented for caldera structures.

Author Contributions

Conceptualization, J.U.-F. and L.P.-C.; methodology, J.A.P.-M., J.U.-F., L.P.-C. and M.E.-R.; software, J.A.P.-M. and M.E.-R.; validation, J.A.P.-M., M.E-R., J.U.-F. and L.P.-C.; formal analysis, J.A.P.-M., J.U.-F., L.P.-C. and M.E.-R.; investigation, J.A.P.-M., J.U.-F., L.P.-C. and M.E.-R.; resources, J.U.-F.; data curation, J.A.P.-M. and M.E.-R.; writing—original

draft preparation, J.U.-F.; writing—review and editing, J.A.P.-M., J.U.-F., L.P.-C. and M.E.-R.; visualization, J.A.P.-M. and M.E.-R.; supervision, J.U.-F.; project administration, J.U.-F.; funding acquisition, J.U.-F. and L.P.-C. All authors have read and agreed to the published version of the manuscript.

Funding

This work was supported by UNAM Coordinacion de Plataformas Oceanograficas and Chicxulub Science Foundation. Support for the geophysical survey and logistics was provided by Socorro Navy Station.

Institutional Review Board Statement

Not applicable.

Informed Consent Statement

Not applicable.

Data Availability Statement

Data is stored in the Chicxulub Institute of Advanced Studies data repository. Data is available upon request from interested parties.

Acknowledgments

We acknowledge permits granted by the Mexican Navy of the Revillagigedo Archipelago to conduct the geophysical studies in Socorro Island. We thank the support provided by the Navy Commander and the Naval Station crew for the geophysical survey. We thank the assistance provided by the UNAM RV El Puma oceanographic cruise to the Revillagigedo Islands. The study forms part of the Eastern Pacific Geophysical Research Program. We thank Marysol Valdez, Rafael Venegas, Osvaldo Sanchez Zamora, and Miguel Angel Diaz for assistance with the project. We acknowledge support from the UNAM Coordinacion de Plataformas Oceanograficas and Chicxulub Science Foundation. This is a contribution IICEAC-25-14.

Conflicts of Interest

The authors declare no conflict of interest.

References

[1] Niu, Y., O'Hara, M.J., 2003. Origin of ocean island basalts: A new perspective from petrology, geochemistry, and mineral physics considerations. Journal of Geophysical Research: Solid Earth. 108(B4), 2002JB002048. DOI: https://doi.org/10.1029/2002JB002048

[2] Nabighian, M.N., Ander, M.E., Grauch, V.J.S., et al., 2005. Historical development of the gravity method in exploration. Geophysics. 70(6). DOI: https://doi.org/10.1190/1.2133785

[3] Miller, C.A., Barretto, J., Stagpoole, V., et al., 2022. The integrated history of repeated caldera formation and infill at the Okataina Volcanic Centre: Insights from 3D gravity and magnetic models. Journal of Volcanology and Geothermal Research. 427, 107555. DOI: https://doi.org/10.1016/j.jvolgeores.2022.107555

[4] Riccardi, U., Pivetta, T., Fedele, A., et al., 2025. Continuous Gravity Observations at Campi Flegrei Caldera: An Accurate Assessment of Tidal and Non-Tidal Signals and Implications for Volcano Monitoring. Pure and Applied Geophysics. 182(3), 1047–1074. DOI: https://doi.org/10.1007/s00024-024-03555-4

[5] Gudmundsson, M.T., Högnadóttir, T., 2007. Volcanic systems and calderas in the Vatnajökull region, central Iceland: Constraints on crustal structure from gravity data. Journal of Geodynamics. 43(1), 153–169. DOI: https://doi.org/10.1016/j.jog.2006.09.015

[6] Montesinos, F.G., Arnoso, J., Gómez-Ortiz, D., et al., 2022. Imaging the Volcanic Structures Beneath Gran Canaria Island Using New Gravity Data. Journal of Geophysical Research: Solid Earth. 127(11), e2022JB024863. DOI: https://doi.org/10.1029/2022JB024863

[7] Kitada, K., Kasaya, T., Iwamoto, H., et al., 2025. Submarine volcanic features inferred from magnetic and gravity anomalies off Kume Island, mid-Okinawa Trough. Geophysical Journal International. 242(2), ggaf226. DOI: https://doi.org/10.1093/gji/ggaf226

[8] Chen, B., Huang, Q., Du, J., et al., 2024. The 3-D Density Structure of the Large Shield Volcanic Structure in the Gardner Region Revealed by a New Gravity Inversion. Geophysical Research Letters. 51(15), e2024GL108667. DOI: https://doi.org/10.1029/2024GL108667

[9] Watts, A.B., Grevemeyer, I., 2025. Legacy Seis-

mic and Gravity Data in the Vicinity of Great Meteor Seamount and Its Tectonic Implications. Journal of Geophysical Research: Solid Earth. 130(5), e2024JB030016. DOI: https://doi.org/10.1029/2024JB030016

[10] Klitgord, K.D., Mammerickx, J., 1982. Northern East Pacific Rise: Magnetic anomaly and bathymetric framework. Journal of Geophysical Research: Solid Earth. 87(B8), 6725–6750. DOI: https://doi.org/10.1029/JB087iB08p06725

[11] Mammerickx, J., Naar, D.F., Tyce, R.L., 1988. The mathematician paleoplate. Journal of Geophysical Research: Solid Earth. 93(B4), 3025–3040. DOI: https://doi.org/10.1029/JB093iB04p03025

[12] Ito, G., Lin, J., Graham, D., 2003. Observational and theoretical studies of the dynamics of mantle plume–mid-ocean ridge interaction. Reviews of Geophysics. 41(4), 2002RG000117. DOI: https://doi.org/10.1029/2002RG000117

[13] Harðardóttir, S., Jackson, M.G., 2025. A new geochemical database for ocean island basalts: Inferring an OIB mantle source from unevenly sampled oceanic hotspots. Chemical Geology. 672, 122505. DOI: https://doi.org/10.1016/j.chemgeo.2024.122505

[14] Ubide, T., Larrea, P., Becerril, L., et al., 2022. Volcanic plumbing filters on ocean-island basalt geochemistry. Geology. 50(1), 26–31. DOI: https://doi.org/10.1130/G49224.1

[15] White, W.M., 2010. Oceanic Island Basalts and Mantle Plumes: The Geochemical Perspective. Annual Review of Earth and Planetary Sciences. 38(1), 133–160. DOI: https://doi.org/10.1146/annurev-earth-040809-152450

[16] Bryan, W.B., 1966. History and mechanism of eruption of soda-rhyolite and alkali basalt, Socorro Island, Mexico. Bulletin Volcanologique. 29(1), 453–479. DOI: https://doi.org/10.1007/BF02597169

[17] Batiza, R., Vanko, D.A., 1985. Petrologic Evolution of Large Failed Rifts in the Eastern Pacific: Petrology of Volcanic and Plutonic Rocks from the Mathematician Ridge Area and the Guadalupe Trough. Journal of Petrology. 26(3), 564–602. DOI: https://doi.org/10.1093/petrology/26.3.564

[18] Bohrson, W.A., Reid, M.R., 1995. Petrogenesis of alkaline basalts from Socorro Island, Mexico: Trace element evidence for contamination of ocean island basalt in the shallow ocean crust. Journal of Geophysical Research: Solid Earth. 100(B12), 24555–24576. DOI: https://doi.org/10.1029/95JB01483

[19] Sclater, J.G., Anderson, R.N., Bell, M.L., 1971. Elevation of ridges and evolution of the central eastern Pacific. Journal of Geophysical Research. 76(32), 7888–7915. DOI: https://doi.org/10.1029/JB076i032p07888

[20] Mammerickx, J., Klitgord, K.D., 1982. Northern East Pacific Rise: Evolution from 25 m.y. B.P. to the present. Journal of Geophysical Research: Solid Earth. 87(B8), 6751–6759. DOI: https://doi.org/10.1029/JB087iB08p06751

[21] Richards, A.F., 1959. Geology of the Islas Revillagigedo, Mexico. Bulletin Volcanologique. 22(1), 73–123. DOI: https://doi.org/10.1007/BF02596580

[22] Maldonado-Koerdell, M., 1958. Barcena Volcano on San Benedicto Island, Revillagigedo Archipelago (Mexico). Ciencia. 18, 114–123. (in Spanish)

[23] Farmer, J.D., Farmer, M.C., Berger, R., 1993. Radiocarbon Ages of Lacustrine Deposits in Volcanic Sequences of the Lomas Coloradas Area, Socorro Island, Mexico. Radiocarbon. 35(2), 253–262. DOI: https://doi.org/10.1017/S0033822200064924

[24] Bohrson, W.A., Reid, M.R., Grunder, A.L., et al., 1996. Prolonged history of silicic peralkaline volcanism in the eastern Pacific Ocean. Journal of Geophysical Research: Solid Earth. 101(B5), 11457–11474. DOI: https://doi.org/10.1029/96JB00329

[25] Batiza, R., 1982. Abundances, distribution and sizes of volcanoes in the Pacific Ocean and implications for the origin of non-hotspot volcanoes. Earth and Planetary Science Letters. 60(2), 195–206. DOI: https://doi.org/10.1016/0012-821X(82)90003-6

[26] Chase, T.E., Menard, H.W., 1968. Four fracture zones off Mexico. In Proceedings of the Pan-American Symposium Upper on the Upper Mantle, Mexico City, Mexico, March 1968; pp. 7–14.

[27] Cole, J., Milner, D., Spinks, K., 2005. Calderas and caldera structures: A review. Earth-Science Reviews. 69(1–2), 1–26. DOI: https://doi.org/10.1016/j.earscirev.2004.06.004

[28] Acocella, V., 2007. Understanding caldera structure and development: An overview of analogue models compared to natural calderas. Earth-Science Reviews. 85(3–4), 125–160. DOI: https://doi.org/10.1016/j.earscirev.2007.08.004

[29] Marti, J., Gudmundsson, A., 2000. The Las Cañadas caldera (Tenerife, Canary Islands): An overlapping collapse caldera generated by magma-chamber migration. Journal of Volcanology and Geothermal Research. 103(1–4), 161–173. DOI: https://doi.org/10.1016/S0377-0273(00)00221-3

[30] Acocella, V., Korme, T., Salvini, F., et al., 2003. Elliptic calderas in the Ethiopian Rift: Control of pre-existing structures. Journal of Volcanology and Geothermal Research. 119(1–4), 189–203. DOI: https://doi.org/10.1016/S0377-0273(02)00342-6

[31] Jellinek, A.M., DePaolo, D.J., 2003. A model for the origin of large silicic magma chambers: Precursors

of caldera-forming eruptions. Bulletin of Volcanology. 65(5), 363–381. DOI: https://doi.org/10.1007/s00445-003-0277-y

[32] Sbarbori, E., Tauxe, L., Goguitchaichvili, A., et al., 2009. Paleomagnetic behavior of volcanic rocks from Isla Socorro, Mexico. Earth, Planets and Space. 61(1), 191–204. DOI: https://doi.org/10.1186/BF03352899

[33] Pavon-Moreno, J.A., Escorza-Reyes, M., Perez-Cruz, L., et al., 2009. Gravity survey of Socorro Island, Revillagigedo Archipelago, Eastern Pacific Ocean. In Proceedings of the American Geophysical Union Spring Meeting, San Francisco, CA, USA, 14–18 December 2009.

[34] Escorza-Reyes, M., Pavon-Moreno, J.A., Perez-Cruz, L., et al., 2009. Volcanic Structure of the Basaltic Shield Volcano of Socorro Island, Mathematician Ridge, Pacific Plate. In Proceedings of the American Geophysical Union Spring Meeting, San Francisco, CA, USA, 14–18 December 2009.

[35] Paoletti, V., Gruber, S., Varley, N., et al., 2016. Insights into the Structure and Surface Geology of Isla Socorro, Mexico, from Airborne Magnetic and Gamma-Ray Surveys. Surveys in Geophysics. 37(3), 601–623. DOI: https://doi.org/10.1007/s10712-015-9352-0

[36] Tapia, C., Yutsis, V., Varley, N., 2021. Crustal structure and magmatic system of Isla Socorro (Eastern Pacific Ocean), derived from the interpretation of geological–geophysical data. Acta Geophysica. 69(6), 2051–2067. DOI: https://doi.org/10.1007/s11600-021-00652-z

[37] Hinze, W.J., Aiken, C., Brozena, J., et al., 2005. New standards for reducing gravity data: The North American gravity database. Geophysics. 70(4), J25–J32. DOI: https://doi.org/10.1190/1.1988183

[38] Holom, D.I., Oldow, J.S., 2007. Gravity reduction spreadsheet to calculate the Bouguer anomaly using standardized methods and constants. Geosphere. 3(2), 86. DOI: https://doi.org/10.1130/GES00060.1

[39] Hinze, W.J., 2003. Bouguer reduction density, why 2.67? Geophysics. 68(5), 1559–1560. DOI: https://doi.org/10.1190/1.1620629

[40] Hurtado-Cardador, M., Urrutia-Fucugauchi, J., 2006. Data reduction and tying in regional gravity surveys—Results from a new gravity base station network and the Bouguer gravity anomaly map for northeastern Mexico. Journal of Geophysics and Engineering. 3(4), 329–337. DOI: https://doi.org/10.1088/1742-2132/3/4/004

[41] Urrutia-Fucugauchi, J., Flores-Ruiz, J.H., 1996. Bouguer Gravity Anomalies and Regional Crustal Structure in Central Mexico. International Geology Review. 38(2), 176–194. DOI: https://doi.org/10.1080/00206819709465330

[42] National Institute of Statistics and Geography (INEGI), 2008. Topographic Map of Socorro Island. INEGI Map: Mexico City, Mexico.

[43] Telford, W.M., Geldart, L.P., Sheriff, R.E., 1995. Applied Geophysics, 2nd ed. Cambridge University Press: New York, NY, USA.

[44] Valdez-Casillas, D.C., Urrutia-Fucugauchi, J., Pérez-Cruz, L., et al., 2024. Gravity and magnetic study of the Xitle volcanic field, Basin of Mexico—Inferences on the pre-eruptive topography. Journal of South American Earth Sciences. 148, 105193. DOI: https://doi.org/10.1016/j.jsames.2024.105193

[45] Blakely, R.J., 1995. Potential Theory in Gravity and Magnetic Applications. Cambridge University Press: Cambridge, UK.

[46] Nava-Flores, M., Ortiz-Alemán, C., Urrutia-Fucugauchi, J., 2023. High Resolution Model of the Vinton Salt-Dome Cap Rock by Joint Inversion of the Full Tensor Gravity Gradient Data with the Simulated Annealing Global Optimization Method. Pure and Applied Geophysics. 180(3), 983–1014. DOI: https://doi.org/10.1007/s00024-023-03227-9

[47] Urrutia-Fucugauchi, J., Arellano-Catalán, O., Pérez-Cruz, L., et al., 2022. Chicxulub Crater Joint Gravity and Magnetic Anomaly Analysis: Structure, Asymmetries, Impact Trajectory and Target Structures. Pure and Applied Geophysics. 179(8), 2735–2756. DOI: https://doi.org/10.1007/s00024-022-03074-0

[48] Liu, Q., Schmidt, M., Sánchez, L., et al., 2024. High-resolution regional gravity field modeling in data-challenging regions for the realization of geopotential-based height systems. Earth, Planets and Space. 76(1), 35. DOI: https://doi.org/10.1186/s40623-024-01981-1

[49] Talwani, M., Worzel, J.L., Landisman, M., 1959. Rapid gravity computations for two-dimensional bodies with application to the Mendocino submarine fracture zone. Journal of Geophysical Research. 64(1), 49–59. DOI: https://doi.org/10.1029/JZ064i001p00049

[50] Rasmussen, R., Pedersen, L.B., 1979. End Corrections in Potential Field Modeling. Geophysical Prospecting. 27(4), 749–760. DOI: https://doi.org/10.1111/j.1365-2478.1979.tb00994.x

[51] Scarponi, M., Hetényi, G., Baron, L., et al., 2022. A gravimetric assessment of the Gotthard Base Tunnel geological model: Insights from a novel gravity terrain-adaptation correction and rock physics data. Swiss Journal of Geosciences. 115(1), 22. DOI: https://doi.org/10.1186/s00015-022-00422-z

[52] Nsiah Ababio, A., Tenzer, R., 2024. A detailed rock density model of the Hong Kong territories. Geodesy and Geodynamics. 15(1), 75–81. DOI: ht

tps://doi.org/10.1016/j.geog.2023.05.006

[53] Ortíz-Alemán, J.C., Negrete-Juarez, R., Urrutia-Fucugauchi, J., et al., 2025. Geophysical Modeling of Complex Karst Features in the Yucatán Peninsula. Pure and Applied Geophysics. 1–25. DOI: https://doi.org/10.1007/s00024-025-03892-y

[54] Somr, M., Žák, J., Kabele, P., et al., 2023. Analysis of fracturing processes leading to caldera collapse. Earth-Science Reviews. 241, 104413. DOI: https://doi.org/10.1016/j.earscirev.2023.104413

[55] Mahood, G.A., 1984. Pyroclastic rocks and calderas associated with strongly peralkaline magmatism. Journal of Geophysical Research: Solid Earth. 89(B10), 8540–8552. DOI: https://doi.org/10.1029/JB089iB10p08540

[56] Colby, D.J., Pyle, D.M., Fontijn, K., et al., 2024. Magma storage conditions beneath a peralkaline caldera in the Main Ethiopian Rift. Journal of Volcanology and Geothermal Research. 455, 108165. DOI: https://doi.org/10.1016/j.jvolgeores.2024.108165

[57] Walker, G.P.L., 1988. Three Hawaiian calderas: An origin through loading by shallow intrusions? Journal of Geophysical Research: Solid Earth. 93(B12), 14773–14784. DOI: https://doi.org/10.1029/JB093iB12p14773

[58] Sanjo, R., Sugai, T., 2025. The spatiotemporal development of downsag and trapdoor structures during caldera subsidence with 1–10 km in diameter in analogue sandbox experiments. Journal of Volcanology and Geothermal Research. 461, 108294. DOI: https://doi.org/10.1016/j.jvolgeores.2025.108294

[59] Acocella, V., Galetto, F., Amelung, F., et al., 2025. Sierra Negra, Galápagos: A resurgent-block basaltic caldera. Geological Society of America Bulletin. 137(3–4), 1703–1716. DOI: https://doi.org/10.1130/B37799.1

[60] Corbi, F., Rivalta, E., Pinel, V., et al., 2015. How caldera collapse shapes the shallow emplacement and transfer of magma in active volcanoes. Earth and Planetary Science Letters. 431, 287–293. DOI: https://doi.org/10.1016/j.epsl.2015.09.028

[61] Morgan, C.L., 2017. Resource estimates of the Clarion-Clipperton manganese nodule deposits. In: Cronan, D.S. (Ed.). Handbook of Marine Mineral Deposits, 1st ed. Routledge: London, UK. pp. 145–170.

[62] Li, J., Jin, Y., Wang, H., et al., 2024. *In-situ* analysis of polymetallic nodules from the Clarion-Clipperton zone, Pacific Ocean: Implication for controlling on chemical composition variability. Frontiers in Marine Science. 11, 1489184. DOI: https://doi.org/10.3389/fmars.2024.1489184

[63] Amon, D.J., Ziegler, A.F., Dahlgren, T.G., et al., 2016. Insights into the abundance and diversity of abyssal megafauna in a polymetallic-nodule region in the eastern Clarion-Clipperton Zone. Scientific Reports. 6(1), 30492. DOI: https://doi.org/10.1038/srep30492

[64] Uhlenkott, K., Meyn, K., Vink, A., et al., 2023. A review of megafauna diversity and abundance in an exploration area for polymetallic nodules in the eastern part of the Clarion Clipperton Fracture Zone (North East Pacific), and implications for potential future deep-sea mining in this area. Marine Biodiversity. 53(2), 22. DOI: https://doi.org/10.1007/s12526-022-01326-9

[65] Barckhausen, U., Bagge, M., Wilson, D.S., 2013. Seafloor spreading anomalies and crustal ages of the Clarion-Clipperton Zone. Marine Geophysical Research. 34(2), 79–88. DOI: https://doi.org/10.1007/s11001-013-9184-6